Editors' Suggestion

Topological Phase Transitions in Disordered Electric Quadrupole Insulators

Chang-An Li,[1,2,‡] Bo Fu,[3] Zi-Ang Hu,[3] Jian Li,[1,2,*] and Shun-Qing Shen[3,†]
[1]School of Science, Westlake University, 18 Shilongshan Road, Hangzhou 310024, Zhejiang Province, China
[2]Institute of Natural Sciences, Westlake Institute for Advanced Study, 18 Shilongshan Road, Hangzhou 310024, Zhejiang Province, China
[3]Department of Physics, The University of Hong Kong, Pokfulam Road, Hong Kong, China

(Received 2 August 2020; revised 10 September 2020; accepted 11 September 2020; published 15 October 2020)

We investigate disorder-driven topological phase transitions in quantized electric quadrupole insulators in two dimensions. We show that chiral symmetry can protect the quantization of the quadrupole moment q_{xy}, such that the higher-order topological invariant is well defined even when disorder has broken all crystalline symmetries. Moreover, nonvanishing q_{xy} and consequent corner modes can be induced from a trivial insulating phase by disorder that preserves chiral symmetry. The critical points of such topological phase transitions are marked by the occurrence of extended boundary states even in the presence of strong disorder. We provide a systematic characterization of these disorder-driven topological phase transitions from both bulk and boundary descriptions.

DOI: 10.1103/PhysRevLett.125.166801

Introduction.—Disorder is ubiquitous in condensed matter systems. A wide range of fundamental phenomena, such as the Anderson localization and the Kondo effect [1–6], are closely related to disordered systems. When disorder is included in the study of topological phases of matter [7,8], the surprising phenomenon of topological Anderson insulators will occur [9–14], which showcases a nontrivial interplay between disorder and topology. Recently, the concept of topological invariants in solids has been generalized to higher orders [15–43]. These higher-order topological insulators, like their conventional cousins, possess boundary states dictated by bulk topological invariants, but only at even lower dimensions than the latter. Among the higher-order topological phases, the quantized electric quadrupole insulator (QEQI) is a prototypical one that features a quantized electric quadrupole moment in the bulk and zero-energy modes at the corners [15,16]. From the outset, a QEQI has been considered as a topological crystalline insulator [44,45], where the quantization of its electric quadrupole moment is protected by the underlying crystalline symmetries [16]. This apparently poses a no-go condition for the existence of any nontrivial effect induced by disorder in such a system, where all the crystalline symmetries are bound to be broken. As such, a systematic study of the disorder effect in QEQIs, especially its resultant topological phase transitions, remains an open problem despite some related efforts [46–53].

In this Letter, we first prove that the electric quadrupole moment will remain quantized in the presence of disorder, as long as a chiral symmetry is preserved in the system. This allows us to investigate well-defined topological phases in disordered QEQIs. We found that disorder generically introduces a deformation of the phase diagram from the clean limit of a QEQI [see Fig. 1(a)]. This deformation is nontrivial in the sense that the topological phase regime can expand due to disorder in certain parameter space [see Fig. 1(b)]. The disordered phase diagrams can be analyzed accurately by using the effective medium theory for the bulk, despite the fact that the topological phase transitions bear no signature in the bulk energy spectrum. Indeed, as an unusual feature of higher-order topological phases, a disorder-induced transition between distinct phases is marked by a localization-delocalization-localization (LDL) transition on specific

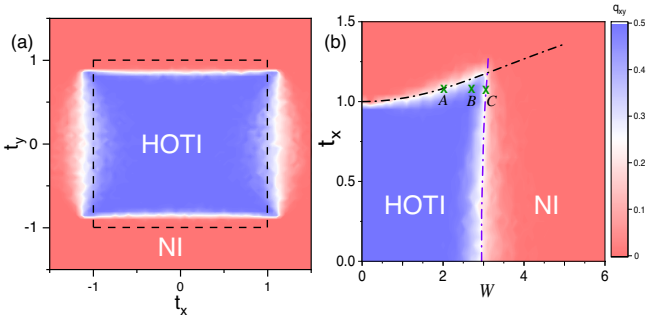

FIG. 1. Phase diagrams of disordered electric quadrupole insulators. (a) Electric quadrupole moment q_{xy} as a function of mass parameters t_x and t_y at a fixed disorder strength $W = 2.5$. The dashed lines indicate the phase boundaries in the clean limit. (b) q_{xy} as a function of t_x and W at fixed $t_y = 0.8$. The dot-dashed lines are the phase boundaries obtained from an effective medium theory. In these phase diagrams, the disorder is of the $V(\mathbf{r})\gamma_4$ type, with 120/150 random configurations averaged in (a)/(b). The system is of size $L_x \times L_y = 30 \times 30$ with periodical boundary conditions. The two distinct phases are higher-order topological insulator and normal insulator.

parts of the system boundary, which leads to a redistribution of fractional charges at the corners of a QEQI. We demonstrate this picture explicitly by combining finite-size scaling analyses with exactly obtained charge densities.

Quantized electric quadrupole moments q_{xy} protected by chiral symmetry.—We consider the following effective Bloch Hamiltonian for a QEQI [15,16]:

$$H_q(\mathbf{k}) = t\sin k_y\gamma_1 + [t_y + t\cos k_y]\gamma_2 + t\sin k_x\gamma_3 + [t_x + t\cos k_x]\gamma_4, \quad (1)$$

where the gamma matrices are defined as $\gamma_j = -\tau_2\sigma_j$ ($j = 1, 2, 3$) and $\gamma_4 = \tau_1\sigma_0$ with τ and σ both being Pauli matrices but for different degrees of freedom; $k_{x/y}$ is the wave vector along x/y (we have set the lattice constant to be unit). The bulk bands of Eq. (1) are gapped unless $|t_x| = |t_y| = |t|$. Without loss of generality, we will set $t = 1$ hereafter. This model respects chiral symmetry $\gamma_5^{-1}H_q(\mathbf{k})\gamma_5 = -H_q(\mathbf{k})$, where the chiral symmetry operator $\gamma_5 \equiv -\gamma_1\gamma_2\gamma_3\gamma_4 = \tau_3\sigma_0$. Since k_x and k_y are decoupled in Eq. (1), the total Hamiltonian can be recast as the sum of two Su-Schrieffer-Heeger (SSH) models along two directions as $H_q(\mathbf{k}) = H_x(k_x) + H_y(k_y)$. In the clean limit, the topologically nontrivial phase is constrained in the region $|t_{s=x,y}| < 1$ where both $H_x(k_x)$ and $H_y(k_y)$ are topologically nontrivial. Under this condition, if an open boundary with a right-angle corner is considered, we can solve the corner state wave function to be of the form $\Psi_c(x, y) = \chi_c\phi_x(x)\phi_y(y)$, where ϕ_x and ϕ_y are two scalar functions, and χ_c is an eigenstate of the chiral symmetry operator: $\gamma_5\chi_c = \pm\chi_c$ [54].

When disorder is introduced into the system, the first question we encounter is whether, or when, the electric quadrupole moment will remain quantized, such that a disordered QEQI phase can be well defined. This question is particularly relevant because QEQIs have been constructed as topological crystalline insulators from the outset, where mirror symmetries are required to ensure the quantization of the electric quadrupole moment. In addition, the nested Wilson loop approach [16] originally used to obtain the topological invariant from the momentum space is no longer applicable in the disordered systems. Here, we prove that the quadrupole moment defined in the real space, given by [55,59,60]

$$q_{xy} = \frac{1}{2\pi}\mathrm{Im}\ \log\ [\det(U^\dagger\hat{Q}U)\sqrt{\det(\hat{Q}^\dagger)}], \quad (2)$$

is indeed quantized even in the presence of disorder as long as the chiral symmetry is preserved. In the above equation, $\hat{Q} \equiv \exp[i2\pi\hat{q}_{xy}]$ and $\hat{q}_{xy} \equiv \hat{x}\,\hat{y}\,/(L_xL_y)$ with $\hat{x}(\hat{y})$ the position operator along the $x(y)$ dimension and $L_{x,y}$ the corresponding size; $\sqrt{\det(\hat{Q}^\dagger)} = \exp[-i\pi\mathrm{Tr}\hat{q}_{xy}]$; the matrix U is constructed by column-wise packing all the occupied eigenstates, such that $UU^\dagger$ is the projector to the occupied subspace.

We sketch our proof as follows and leave the full details in the Supplemental Material [54]. For q_{xy} to be quantized as an integer multiple of $1/2$, clearly $\det(U^\dagger\hat{Q}U)\sqrt{\det\hat{Q}^\dagger}$ has to be real. By using Sylvester's determinant identity $\det(\mathbf{1} + AB) = \det(\mathbf{1} + BA)$, and the identity $UU^\dagger + VV^\dagger = \mathbf{1}$ with $VV^\dagger$ the projector to the unoccupied subspace (V is constructed from the unoccupied eigenstates similar to U), we obtain $\det(U^\dagger\hat{Q}U) = \det(V^\dagger\hat{Q}^\dagger V)\det\hat{Q}$. Noticing that the chiral symmetry operator relates the occupied states with unoccupied states by $V = \gamma_5 U$, as well as the fact that $[\gamma_5, \hat{Q}] = 0$, we have

$$\det(U^\dagger\hat{Q}U) = \det(U^\dagger\hat{Q}^\dagger U)\det\hat{Q}. \quad (3)$$

Since $\hat{Q}$ is unitary, it follows immediately that $\det(U^\dagger\hat{Q}U)\sqrt{\det Q^\dagger}$ is real. In other words, q_{xy} is quantized to be 0 or $1/2$ as long as the system preserves the chiral symmetry [54]. Note that, in this proof, the explicit form of $\hat{Q}$ is irrelevant except for its commutativity with the chiral symmetry operator, which is generally true because the chiral symmetry is a local symmetry (i.e., diagonal in terms of real-space degrees of freedom) whereas $\hat{Q}$ is constructed from position operators only. Therefore, the conclusion of this proof can be straightforwardly generalized by replacing $\hat{Q}$ with other functions of position operators such as the electric octupole moment operator [15,16]. In the Supplemental Material [54], we further show how to generalize this proof to the case of particle-hole symmetry [60], which is also a local symmetry but does not commute with $\hat{Q}$ because of its antiunitary nature.

Phase diagram of disordered electric quadrupole insulators.—With a well-defined topological invariant established for disordered QEQIs, we now present the resulting phase diagrams based on the model in Eq. (1). To be specific, we choose one particular type of disorder that preserves the chiral symmetry, represented by $V_{\mathrm{dis}} = V(\mathbf{r})\gamma_4$ with the random function $V(\mathbf{r})$ distributed uniformly within the interval $[-W/2, W/2]$ and W being the disorder strength. The averaged quadrupole moment q_{xy} of disordered QEQIs as a function of t_x and t_y is shown in Fig. 1(a). Two separate phases can be clearly distinguished: one with $q_{xy} = 1/2$ (in blue) signifying a nontrivial higher-order topological insulator (HOTI) phase, and the other with $q_{xy} = 0$ (in red) signifying a trivial normal insulator (NI) phase. This phase diagram is more informative when compared with the phase diagram in the clean limit, the phase boundary of which has been marked by dashed lines also in Fig. 1(a). There are obviously contrasting behaviors in terms of the deformation of the HOTI phase regime in the two parameter dimensions (t_x and t_y) caused by disorder: the HOTI phase occurs in a shrunk range in t_y but an expanded range in t_x—the chosen type of disorder is

coupled to the same gamma matrix γ_4 with the latter parameter but not the former one. A more precise analysis of how the deformed phase boundary relies on the disorder type and strength will be given in the next section by employing the effective medium theory and the self-consistent Born approximation (SCBA). Before that, we examine more closely the disorder induced expansion of the nontrivial HOTI phase in the parameter space t_x.

In Fig. 1(b) we show the phase diagram in the W-t_x space with fixed t_y. We notice again two types of phase boundaries, marked by a black (upper) and a purple (right side) dot-dashed line, respectively. The upper phase boundary exhibits a clear monotonic increase of the critical t_x with stronger disorder W, corresponding to the expanded t_x range by disorder for the HOTI phase in Fig. 1(a), until it intersects with the right-side phase boundary. As we are set to show in the next section, the right-side phase boundary, which puts an upper bound of the disorder strength for the HOTI phase, originates from the constraint imposed by the disorder-renormalized t_y that has also led to the shrunk range of t_y for the HOTI phase in Fig. 1(a). These two phase boundaries represent exactly the topological phase transitions that are central to this paper.

Effective medium theory of the disorder-induced topological phase transitions.—A better understanding of the disorder-induced topological phase transitions can be achieved with the help of an effective medium theory and the SCBA method [61–64]. In the SCBA method, the key is to obtain the self-energy introduced by the disorder self-consistently, and then to include the self-energy as renormalization to the original Hamiltonian. In our case, by symmetry arguments the self-energy can be simplified to be

$$\Sigma(E_F) = \Sigma_4\gamma_4 + \Sigma_2\gamma_2 + \Sigma_0 I_{4\times 4}. \tag{4}$$

Specifically, the self-energy Σ satisfies the following self-consistent integral equation:

$$\Sigma(E_F) = \frac{W^2}{48\pi^2}\int_{BZ} d^2\mathbf{k}\gamma_4 \frac{1}{E_F + i\eta - H_q(\mathbf{k}) - \Sigma(E_F)}\gamma_4, \tag{5}$$

where the integral runs over the first Brillouin zone, and η is an infinitesimal positive number. E_F is Fermi energy which is set at zero here, i.e., the system is half filled. From Eq. (5), there are explicitly three coupled self-consistent integral equations that will fully determine Σ [54]. After obtaining the self-energy Σ (where Σ_0 turns out to be zero at zero energy because of the chiral symmetry), the topological mass terms t_x and t_y are renormalized according to

$$\bar{t}_x = t_x + \mathrm{Re}\Sigma_4, \tag{6a}$$

$$\bar{t}_y = t_y + \mathrm{Re}\Sigma_2. \tag{6b}$$

This produces the new phase boundaries at $|\bar{t}_x| = |\bar{t}_y| = 1$, which formally resemble the conditions in the clean limit but with a key difference in the implicit dependence on W.

The preceding approach can quantitatively account for the phase boundaries in the presence of disorder. The expanded range of t_x and the shrunk range of t_y for the HOTI phase in the disordered phase diagram, as shown in Fig. 1(a), can be understood from the opposite signs of the self-energy contributions Σ_4 and Σ_2, which in turn comes from the anticommutation relation between γ_4 and γ_2 [54]. In previous discussions, we have seen that only if the two individual SSH models consisting the full model in Eq. (1) are topologically nontrivial simultaneously, the system can possess nontrivial bulk topological invariant and host zero-energy modes at its corners. Therefore, if disorder drives one of the two SSH components from topologically nontrivial to trivial, a phase transition of the higher-dimensional system will occur. Indeed, the topological phase transitions of the two SSH components are each captured by one of the conditions $|\bar{t}_{x,y}| = 1$ with the renormalized mass $\bar{t}_{x,y}(t_{x,y}, W)$ given by Eq. (6). For a fixed disorder strength W, such as in the case shown in Fig. 1(a), these conditions lead to four critical values of t_x and t_y, resulting in a rectangular shaped phase boundary in the phase diagram. With varying disorder strength, on the other hand, the two conditions lead directly to the two phase boundary lines demonstrated in Fig. 1(b). Specifically, we plot the solutions to the equations $\bar{t}_x = 1$ and $\bar{t}_y = 1$ as the dot-dashed lines in black and in purple, respectively. Both lines coincide very well with the phase boundaries obtained from numerically calculating q_{xy} as discussed in previous sections, until the two lines intersect.

Localization-delocalization-localization transitions at open boundaries.—The higher-order topological phase transitions generically show no signatures in terms of the bulk energy spectrum but instead are accompanied by LDL transitions at the open boundaries of the system. To demonstrate this in disordered systems, we perform a finite size scaling analysis based on localization length calculated from the numerical transfer matrix method [54,65–67]. Specifically, we compare the localization length (at zero energy) along quasi-one-dimensional ribbons of our model system with different width, longitudinal orientations, and transverse boundary conditions. The dependence of the localization length on the ribbon width, in a specific orientation and boundary condition setting, indicates the presence or absence of delocalized bulk or boundary states in the thermodynamic limit. We focus on the parameter space close to the phase boundaries identified in the previous sections. With a periodic boundary condition in the transverse dimension, we found that the localization length (upon normalization by the width) decrease monotonically with increasing width in the entire parameter ranges of our interest, regardless of the orientation along the ribbon [54]. This indicates that there is no occurrence of

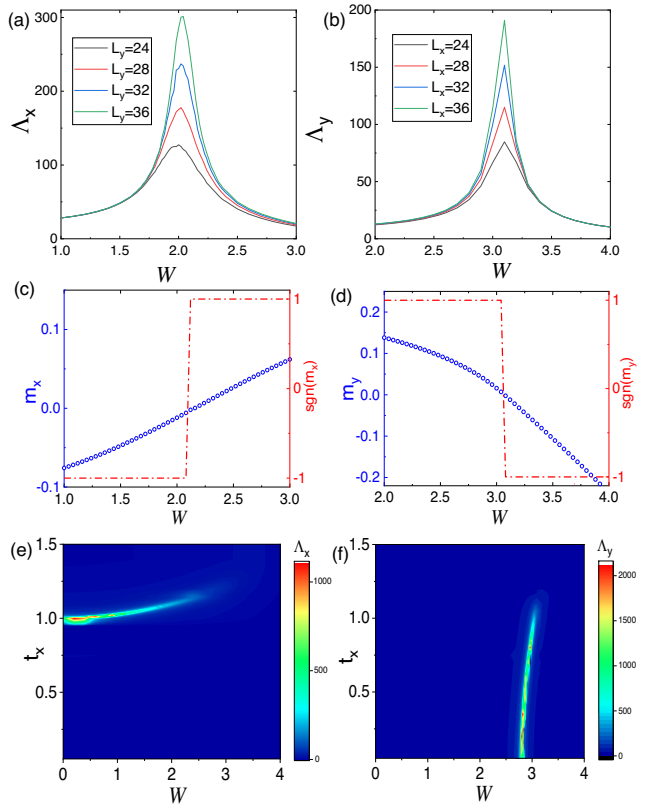

FIG. 2. Signatures of delocalized states at the open boundaries: a finite-size scaling analysis of the localization length (a) Λ_x and (b) Λ_y as functions of W with an open boundary condition in the transverse dimension; effective boundary mass terms (c) m_x and (d) m_y as functions of W; phase boundaries indicated by the divergence of (e) Λ_x and (f) Λ_y as analyzed in (a),(b). In (a)–(d), we have set $t_x = 1.1$ and $t_y = 0.8$.

delocalized bulk states during the phase transitions—the bulk of the system remains insulating. In contrast, when an open boundary condition is considered, the localization length along certain longitudinal orientation can exhibit monotonic increase with increasing width, signifying a divergence in the thermodynamic limit, around a topological phase transition point, as exemplified in Figs. 2(a) and 2(b). The divergence of the localization length at a critical value of the disorder strength, which occurs only with an open boundary condition and along certain orientation, indicates the existence of delocalized states at the corresponding boundaries, despite strong disorder, at the critical point. We note that the LDL transitions discussed here are similar to the topological phase transitions across Landau levels in the quantum Hall effect [68], in the fact that the delocalized states occur only at the exact critical points.

The boundary LDL transitions established above by a finite-size scaling analysis can be further understood with an effective boundary theory [54], where the (boundary) spectrum around a critical point is controlled by an effective mass, given by $m_x = 1 - t_x - \mathrm{Re}[\Sigma_4(W)]$ for the boundaries along x, or $m_y = 1 - t_y - \mathrm{Re}[\Sigma_2(W)]$ for the boundaries along y. The critical points are associated with the conditions $m_{x,y} = 0$, which coincide with the conditions that we have derived earlier from the bulk phase transitions. By using the SCBA method, the effective mass values and corresponding signs are obtained and shown in Figs. 2(c) and 2(d), which agree with the finite-size scaling results.

The LDL transitions along each open boundary orientation also enable us to establish the two types of phase boundaries discussed previously in the context of bulk topology. This is shown in Figs. 2(e) and 2(f) with calculated localization length corresponding to Figs. 2(a) and 2(b). The full agreement between this approach and the bulk invariant approach manifests the close interconnection between the boundary and the bulk descriptions of the higher-order topological phase transitions.

Charge density redistribution at boundaries and corners.—A hallmark of QEQIs is the presence of fractional charges at the corners which consist in the quantized electric quadrupole. In this section we demonstrate how the disorder-driven topological phase transitions lead to the redistribution of the charge density towards (or away from) the fractional corner charges. For clarity and simplicity, let us focus on three representative points in the phase diagram, marked by A, B, and C in Fig. 1(b). These three phase points correspond to a fixed t_x (we choose $t_x = 1.1$) but varying disorder strength W, such that A and C sit on the two types of phase boundaries respectively, whereas B sits in the nontrivial QEQI phase. The calculated charge densities for these points are shown in Fig. 3. At the critical point $A(C)$, the charge density extends only along the $x(y)$ boundaries, as enabled by the occurrence of delocalized states thereat, and exhibits a continuous bipolar form with opposite polarities (offset by the mean values) on opposite boundaries; at the B point, the charge density displays a more symmetric quadrupolar form that is deformed from the dipoles in A or C. The charge density in the B point shows clear localization at the corners owing to the topological bulk-corner correspondence, and upon integration over each quadrant sums to the fractional

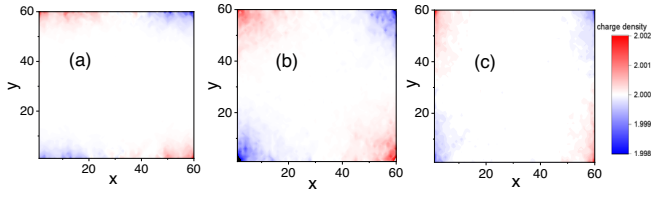

FIG. 3. Charge density distributions (a)–(c) that correspond to the three points, A, B, and C (marked by crosses) in the phase diagram in Fig. 1(b). The points A and C sit in different phase boundaries; the point B sits inside the nontrivial QEQI phase. The values of the disorder strength in (a)–(c) are $W = 2.02$, $W = 2.70$, and $W = 3.10$, respectively. In all these calculations we have set $t_x = 1.1$ and $t_y = 0.8$, and taken an average of 10 disorder configurations.

value $\pm 1/2$ with high accuracy when the system size is sufficiently large.

Conclusion.—In short, we have presented a comprehensive description of the disorder-induced topological phase transitions in quantized electric quadrupole insulators. It is proved rigorously that the quantization of the electric quadrupole moment q_{xy} can be protected by the chiral symmetry even in the presence of strong disorder. We have also uncovered disorder-driven phase transitions from trivial to higher-order topological phases, which are signified by localization-delocalization-localization transitions at certain open boundaries with the system bulk remaining insulating. We expect this exotic disorder effect can be experimentally demonstrated in, e.g., photonic crystals [39–41] or electric circuits [37,38] by taking advantage of their high controllability.

C. A. L. thanks Liyuan Chen and A. Weststrom for helpful discussions, and acknowledges B. Kang and G. Y. Cho for communication on the real part of the quadrupole formula. This work was supported by NSFC under Grant No. 11774317, NSF of Zhejiang under Grant No. LQ20A040003, and the Research Grants Council, University Grants Committee, Hong Kong under Grants No. 17301717 and No. 17301220. The numerical calculations were performed on the supercomputer cluster of Westlake University.

Note added.—We came to notice related works on arXiv [69–71] upon submission of the present manuscript.

*lijian@westlake.edu.cn
†sshen@hku.hk
‡Present address: Institute of Theoretical Physics and Astrophysics, University of Wurzburg, D-97074 Wurzburg, Germany.

[1] P. A. Lee and T. V. Ramakrishnan, Disordered electronic systems, Rev. Mod. Phys. **57**, 287 (1985).
[2] P. W. Anderson, Absence of diffusion in certain random lattices, Phys. Rev. **109**, 1492 (1958).
[3] F. Evers and A. D. Mirlin, Anderson transitions, Rev. Mod. Phys. **80**, 1355 (2008).
[4] L. Sanchez-Palencia and M. Lewenstein, Disordered quantum gases under control, Nat. Phys. **6**, 87 (2010).
[5] J. Kondo, Resistance minimum in dilute magnetic alloys, Prog. Theor. Phys. **32**, 37 (1964).
[6] A. C. Hewson, *The Kondo Problem to Heavy Fermions* (Cambridge University Press, Cambridge, England, 1997).
[7] M. Z. Hasan and C. L. Kane, Colloquium: Topological insulators, Rev. Mod. Phys. **82**, 3045 (2010).
[8] X.-L. Qi and S.-C. Zhang, Topological insulators and superconductors, Rev. Mod. Phys. **83**, 1057 (2011).
[9] J. Li, R.-L. Chu, J. K. Jain, and S.-Q. Shen, Topological Anderson Insulator, Phys. Rev. Lett. **102**, 136806 (2009).
[10] H. Jiang, L. Wang, Q.-f. Sun, and X. C. Xie, Numerical study of the topological Anderson insulator in HgTe/CdTe quantum wells, Phys. Rev. B **80**, 165316 (2009).
[11] H.-M. Guo, G. Rosenberg, G. Refael, and M. Franz, Topological Anderson Insulator in Three Dimensions, Phys. Rev. Lett. **105**, 216601 (2010).
[12] I. Mondragon-Shem, T. L. Hughes, J. Song, and E. Prodan, Topological Criticality in the Chiral-Symmetric AIII Class at Strong Disorder, Phys. Rev. Lett. **113**, 046802 (2014).
[13] E. J. Meier, F. A. An, A. Dauphin, M. Maffei, P. Massignan, T. L. Hughes, and B. Gadway, Observation of the topological Anderson insulator in disordered atomic wires, Science **362**, 929 (2018).
[14] S. Stutzer, Y. Plotnik, Y. Lumer, P. Titum, N. H. Lindner, M. Segev, M. C. Rechtsman, and A. Szameit, Photonic topological Anderson insulators, Nature (London) **560**, 461 (2018).
[15] W. A. Benalcazar, B. A. Bernevig, and T. L. Hughes, Quantized electric multipole insulators, Science **357**, 61 (2017).
[16] W. A. Benalcazar, B. A. Bernevig, and T. L. Hughes, Electric multipole moments, topological multipole moment pumping, and chiral hinge states in crystalline insulators, Phys. Rev. B **96**, 245115 (2017).
[17] F. Schindler, A. M. Cook, M. G. Vergniory, Z. Wang, S. S. P. Parkin, B. A. Bernevig, and T. Neupert, Higher-order topological insulators, Sci. Adv. **4**, eaat0346 (2018).
[18] J. Langbehn, Y. Peng, L. Trifunovic, F. von Oppen, and P. W. Brouwer, Reflection-Symmetric Second-Order Topological Insulators and Superconductors, Phys. Rev. Lett. **119**, 246401 (2017).
[19] R.-J. Slager, L. Rademaker, J. Zaanen, and L. Balents, Impurity-bound states and Green's function zeros as local signatures of topology, Phys. Rev. B **92**, 085126 (2015).
[20] Y. Peng, Y. Bao, and F. von Oppen, Boundary Green functions of topological insulators and superconductors, Phys. Rev. B **95**, 235143 (2017).
[21] Z. Song, Z. Fang, and C. Fang, $(d-2)$-Dimensional Edge States of Rotation Symmetry Protected Topological States, Phys. Rev. Lett. **119**, 246402 (2017).
[22] E. Khalaf, Higher-order topological insulators and superconductors protected by inversion symmetry, Phys. Rev. B **97**, 205136 (2018).
[23] Y. You, T. Devakul, F. J. Burnell, and T. Neupert, Higher-order symmetry-protected topological states for interacting bosons and fermions, Phys. Rev. B **98**, 235102 (2018).
[24] M. Geier, L. Trifunovic, M. Hoskam, and P. W. Brouwer, Second-order topological insulators and superconductors with an order-two crystalline symmetry, Phys. Rev. B **97**, 205135 (2018).
[25] M. Ezawa, Higher-Order Topological Insulators and Semimetals on the Breathing Kagome and Pyrochlore Lattices, Phys. Rev. Lett. **120**, 026801 (2018).
[26] S. Franca, J. van den Brink, and I. C. Fulga, An anomalous higher-order topological insulator, Phys. Rev. B **98**, 201114 (R) (2018).
[27] R. Okugawa, S. Hayashi, and T. Nakanishi, Second-order topological phases protected by chiral symmetry, Phys. Rev. B **100**, 235302 (2019).
[28] Z. Wang, B. J. Wieder, J. Li, B. Yan, and B. A. Bernevig, Higher-Order Topology, Monopole Nodal Lines, and the

Origin of Large FERMI Arcs in Transition Metal Dichalcogenides XTe_2, Phys. Rev. Lett. **123**, 186401 (2019).
[29] K. Kudo, T. Yoshida, and Y. Hatsugai, Higher-Order Topological Mott Insulators, Phys. Rev. Lett. **123**, 196402 (2019).
[30] M. J. Park, Y. Kim, G. Y. Cho, and S. B. Lee, Higher-Order Topological Insulator in Twisted Bilayer Graphene, Phys. Rev. Lett. **123**, 216803 (2019).
[31] H. Li and K. Sun, Pfaffian Formalism for Higher-Order Topological Insulators, Phys. Rev. Lett. **124**, 036401 (2020).
[32] L. Trifunovic and P. W. Brouwer, Higher-Order Bulk-Boundary Correspondence for Topological Crystalline Phases, Phys. Rev. X **9**, 011012 (2019).
[33] L. Trifunovic and P. W. Brouwer, Higher-order topological band structures, arXiv:2003.01144.
[34] I. Petrides and O. Zilberberg, Higher-order topological insulators, topological pumps and the quantum Hall effect in high dimensions, Phys. Rev. Research **2**, 022049(R) (2020).
[35] F. Schindler, Z. Wang, M. G. Vergniory, A. M. Cook, A. Murani, S. Sengupta, A. Y. Kasumov, R. Deblock, S. Jeon, I. Drozdov, H. Bouchiat, S. Gueon, A. Yazdani, B. A. Bernevig, and T. Neupert, Higher-order topology in bismuth, Nat. Phys. **14**, 918 (2018).
[36] M. Serra-Garcia, V. Peri, R. Sustrunk, O. R. Bilal, T. Larsen, L. G. Villanueva, and S. D. Huber, Observation of a phononic quadrupole topological insulator, Nature (London) **555**, 342 (2018).
[37] C. W. Peterson, W. A. Benalcazar, T. L. Hughes, and G. Bahl, A quantized microwave quadrupole insulator with topologically protected corner states, Nature (London) **555**, 346 (2018).
[38] S. Imhof, C. Berger, F. Bayer, J. Brehm, L. W. Molenkamp, T. Kiessling, F. Schindler, C. H. Lee, M. Greiter, T. Neupert, and R. Thomale, Topolectrical-circuit realization of topological corner modes, Nat. Phys. **14**, 925 (2018).
[39] B.-Y. Xie, G.-X. Su, H.-F. Wang, H. Su, X.-P. Shen, P. Zhan, M.-H. Lu, Z.-L. Wang, and Y.-F. Chen, Visualization of Higher-Order Topological Insulating Phases in Two-Dimensional Dielectric Photonic Crystals, Phys. Rev. Lett. **122**, 233903 (2019).
[40] X.-D. Chen, W.-M. Deng, F.-L. Shi, F.-L. Zhao, M. Chen, and J.-W. Dong, Direct Observation of Corner States in Second-Order Topological Photonic Crystal Slabs, Phys. Rev. Lett. **122**, 233902 (2019).
[41] A. El Hassan, F. K. Kunst, A. Moritz, G. Andler, E. J. Bergholtz, and M. Bourennane, Corner states of light in photonic waveguides, Nat. Photonics **13**, 697 (2019).
[42] X. Ni, M. Weiner, A. Alu, and A. B. Khanikaev, Observation of higher-order topological acoustic states protected by generalized chiral symmetry, Nat. Mater. **18**, 113 (2019).
[43] Y. Qi, C. Qiu, M. Xiao, H. He, M. Ke, and Z. Liu, Acoustic Realization of Quadrupole Topological Insulators, Phys. Rev. Lett. **124**, 206601 (2020).
[44] L. Fu, Topological Crystalline Insulators, Phys. Rev. Lett. **106**, 106802 (2011).
[45] T. Neupert and F. Schindler, Topological crystalline insulators, in *Topological Matter: Lectures from the Topological Matter School 2017*, edited by D. Bercioux, J. Cayssol, M. G. Vergniory, and M. Reyes Calvo (Springer International Publishing, Cham, 2018), pp. 31–61.
[46] R. Chen, C.-Z. Chen, J.-H. Gao, B. Zhou, and D.-H. Xu, Higher-Order Topological Insulators in Quasicrystals, Phys. Rev. Lett. **124**, 036803 (2020).
[47] A. Agarwala, V. Juricic, and B. Roy, Higher-order topological insulators in amorphous solids, Phys. Rev. Research **2**, 012067(R) (2020).
[48] C.-A. Li and S.-S. Wu, Topological states in generalized electric quadrupole insulators, Phys. Rev. B **101**, 195309 (2020).
[49] H. Araki, T. Mizoguchi, and Y. Hatsugai, Phase diagram of a disordered higher-order topological insulator: A machine learning study, Phys. Rev. B **99**, 085406 (2019).
[50] Z. Su, Y. Kang, B. Zhang, Z. Zhang, and H. Jiang, Disorder induced phase transition in magnetic higher-order topological insulator: A machine learning study, Chin. Phys. B **28**, 117301 (2019).
[51] C. H. Lee, S. Imhof, C. Berger, F. Bayer, J. Brehm, L. W. Molenkamp, T. Kiessling, and R. Thomale, Topolectrical Circuits, Commun. Phys. **1**, 39 (2018).
[52] C. Wang and X. R. Wang, Disorder-induced quantum phase transitions in three-dimensional second-order topological insulators, arXiv:2005.06740.
[53] S. Franca, D. V. Efremov, and I. C. Fulga, Phase-tunable second-order topological superconductor, Phys. Rev. B **100**, 075415 (2019).
[54] See Supplemental Material at http://link.aps.org/supplemental/10.1103/PhysRevLett.125.166801, which includes Refs. [55–58], for details of (Sec. S1) proof of the quantization of quadrupole moments protected by chiral symmetry, (Sec. S2) effective low-energy edge Hamiltonian and corner modes solution, (Sec. S3) self-consistent Born approximation, (Sec. S4) signatures of disorder induced nontrivial phase, (Sec. S5) the real part of the quadrupole moment formula, (Sec. S6) finite size scaling result, and (Sec. S7) edge Hamiltonian based on lattice model.
[55] B. Kang, K. Shiozaki, and G. Y. Cho, Many-body order parameters for multipoles in solids, Phys. Rev. B **100**, 245134 (2019).
[56] S.-Q. Shen, *Topological Insulators: Dirac Equation in Condensed Matter*, 2nd ed. (Springer, Singapore, 2017).
[57] R. Resta, Quantum-Mechanical Position Operator in Extended Systems, Phys. Rev. Lett. **80**, 1800 (1998).
[58] R. Resta and S. Sorella, Electron Localization in the Insulating State, Phys. Rev. Lett. **82**, 370 (1999).
[59] W. A. Wheeler, L. K. Wagner, and T. L. Hughes, Many-body electric multipole operators in extended systems, Phys. Rev. B **100**, 245135 (2019).
[60] B. Roy, Antiunitary symmetry protected higher-order topological phases, Phys. Rev. Research **1**, 032048 (2019).
[61] C. W. Groth, M. Wimmer, A. R. Akhmerov, J. Tworzydlo, and C. W. J. Beenakker, Theory of the Topological Anderson Insulator, Phys. Rev. Lett. **103**, 196805 (2009).
[62] M. J. Park, B. Basa, and M. J. Gilbert, Disorder-induced phase transitions of type-II Weyl semimetals, Phys. Rev. B **95**, 094201 (2017).

[63] C.-Z. Chen, J. Song, H. Jiang, Q.-f. Sun, Z. Wang, and X. C. Xie, Disorder and Metal-Insulator Transitions in Weyl Semimetals, Phys. Rev. Lett. **115**, 246603 (2015).

[64] S. Liu, T. Ohtsuki, and R. Shindou, Effect of Disorder in a Three-Dimensional Layered Chern Insulator, Phys. Rev. Lett. **116**, 066401 (2016).

[65] A. MacKinnon and B. Kramer, The scaling theory of electrons in disordered solids: Additional numerical results, Z. Phys. B **53**, 1 (1983).

[66] B. Kramer and A. MacKinnon, Localization: Theory and experiment, Rep. Prog. Phys. **56**, 1469 (1993).

[67] A. Yamakage, K. Nomura, K.-I. Imura, and Y. Kuramoto, Criticality of the metal-insulator transition driven by disorder, Phys. Rev. B **87**, 205141 (2013).

[68] T. Ando, Electron Localization in a Two-Dimensional System in Strong Magnetic Fields. I. Case of Short-Range Scatterers, J. Phys. Soc. Jpn. **52**, 1740 (1983).

[69] A. Coutant, V. Achilleos, O. Richoux, G. Theocharis, and V. Pagneux, Robustness against disorder of topological corner modes and application to acoustic networks, arXiv:2007.13217.

[70] Y.-B. Yang, K. Li, L.-M. Duan, and Y. Xu, Higher-order Topological Anderson Insulators, arXiv:2007.15200.

[71] W. Zhang, D. Zou, Q. Pei, W. He, J. Bao, H.-j. Sun, and X. Zhang, , Experimental Observation of Higher-Order Topological Anderson Insulators, arXiv:2008.00423.